Solvothermal synthesis and electromagnetic absorption properties of pyramidal Ni superstructures

Biao Zhao, Gang Shao, Bingbing Fan, Yajun Xie, and Binbin Wang
School of Materials Science and Engineering, Zhengzhou University, Zhengzhou, Henan 450001, People's Republic of China

Rui Zhang[a)]
School of Materials Science and Engineering, Zhengzhou University, Zhengzhou, Henan 450001, People's Republic of China; and Zhengzhou Aeronautical Institute of Industry Management, Zhengzhou, Henan 450046, People's Republic of China

(Received 2 March 2014; accepted 19 June 2014)

The submicrometer Ni cones have been successfully prepared through a simple solvothermal method in glycerol. The as-prepared products were extensively characterized by x-ray diffraction, field emission scanning electron microscopy, energy-dispersive x-ray spectroscopy, Fourier transform infrared spectroscopy, and thermogravimetric analysis. The effects of the volume ratios of glycerol to water, and the concentration of alkali on morphologies of Ni samples were investigated. The electromagnetic wave absorption properties of Ni cones were evaluated based on the relative complex permeability (μ_r) and permittivity (ε_r). A minimum reflection loss (RL) of −41.6 dB was observed at 4.7 GHz with the thickness of 3.8 mm and the RL values below −10 dB were obtained in the range of 3.9–15.0 GHz with the corresponding thickness of 1.8–3.8 mm. The excellent wave absorption properties of the obtained products are due to the synergic effect of dielectric loss and magnetic loss, geometry effect and unique morphology.

I. INTRODUCTION

With the rapid applications of electromagnetic waves in both civil and military fields, it becomes urgent to design and fabricate microwave absorbers to eliminate the problems of electromagnetic interference (EMI). EMI pollution can induce significant disturbances in relative systems.[1,2] Enormous studies have been attracted to seek suitable electromagnetic wave absorption materials, such as ferrites,[3,4] polymorphous ZnO,[5,6] soft magnetic metal,[7–9] and carbon nanotubes.[10–12] Among the candidates for microwave absorbing materials, metallic soft magnetic materials possess many unique features of large saturation magnetization values, Snoek's limit, Curie temperature, and high relative complex magnetic permeability at high frequency ranges.[7,13,14] Therefore, it is always possible to make thin absorbers using soft magnetic materials as fillers. As one of the typical example of soft magnetic materials, Ni has been attracted great attentions with different structures of micro and/or nanometers in the area of microwave absorption. Gao[15] found that the minimum reflection loss (RL) of Ni nanowires reaches −8.5 dB at 10 GHz and the absorption range under −5 dB is from 8.5 to 12.5 GHz with the sample thickness of 3 mm. Wang[16] synthesized and investigated branchlike and flowerslike Ni samples for microwave absorption purpose. Tong[13] reported octahedral Ni exhibited excellent matching and absorbing properties with a minimum RL value of −37.93 dB at 12.80 GHz. Liu[17] presented that urchinlike Ni owned the minimum RL of −43 dB at about 10 GHz with 2 mm in absorber thickness. The electromagnetic performances of ultrafine Ni fibers were also investigated.[8] It can be found that the morphologies play a vital role on their microwave absorption performances. However, the fabrication processes of the above mentioned materials are complex and costly. To the best of our knowledge, there are no public reports on the preparation of pyramidal nano/microstructures of Ni through a simple solvothermal method.

In this paper, a simple, economic chemical-reduction method was applied to synthesize pyramidal nickel by reduction of $NiCl_2$ with glycerol. It is the first reported of pyramidal nickel obtained with glycerol as solvent and reducer. The growth mechanism of Ni pyramidal structures was discussed. The electromagnetic properties were investigated in the range of 1–18 GHz, and the microwave absorption performance was evaluated according to transmission line theory.

II. EXPERIMENTAL

A. Preparation

All chemicals in this experiment were of analytical grade and without further purification. In a typical procedure,

[a)]Address all correspondence to this author.
e-mail: zhangray@zzu.edu.cn
DOI: 10.1557/jmr.2014.151

 © Materials Research Society 2014

https://doi.org/10.1557/jmr.2014.151 Published online by Cambridge University Press

first, a solution was prepared by dissolving 0.005 mol nickel chloride hexahydrate and 0.09 mol sodium hydroxide in 60 mL glycerol, vigorously stirred for 1 h. Second, the mixture solution was transferred into a Teflon-lined stainless-steel autoclave and maintained at 200 °C for 15 h. When the reaction was completed, dark substances were deposited on the bottom of the Teflon cup. The target products were collected and rinsed with distilled water and ethanol for several times and then dried in a vacuum oven at 60 °C for 12 h. In addition, the effects on the morphologies of nickel samples, such as the types of solvent, time, and concentration of sodium hydroxide, were also considered.

B. Characterization

The structural information of the samples was characterized by a powder x-ray diffraction (XRD) method. Diffraction patterns of intensity versus 2θ were recorded using a XD-3 (Beijing Purkinje General Instrument Co. Ltd., Beijing, China) diffractometer equipped with a Cu K_α radiation source ($\lambda = 0.15418$ nm) from 20° to 80°, which operated at 36 kV and 20 mA. The morphology of the products was observed using field emission scanning electron microscopy (FESEM; ... model JEOL JSM-7001F, Tokyo, Japan) operated at 15 kV. The element composition was carried out by an energy dispersive x-ray spectroscopy (EDS, Oxford Instruments) associated with FESEM. Fourier transform infrared (FTIR) spectra were recorded on a Nicolet iS10 FTIR spectrometer (Tewksbury, MA). The thermogravimetric (TG) was studied by a STA 409/PC simultaneous thermal analyzer (Netzsch, Selb, Germany) from room temperature to 800 °C with a heating rate of 10 °C in flowing air.

The relative permeability ($\mu_r = \mu - j\mu''$) and permittivity ($\varepsilon_r = \varepsilon' - j\varepsilon''$) during 1.0–18.0 GHz were determined via Agilent N5244A vector network analyzer (Santa Clara, CA). A microwave measurement sample containing 70 wt % of Ni cones and 30 wt% wax which was considered as binder was pressed into a ring with the outer diameter of 7.00 mm, the inner diameter of 3.04 mm, and the thickness of 2 mm. The relative complex permittivity ($\varepsilon_r = \varepsilon' - j\varepsilon''$) and permeability ($\mu_r = \mu' - j\mu''$) of the mixture were evaluated in the frequency range of 1–18 GHz by measuring the reflection coefficient S_{11} and the transmission coefficient S_{21}.

III. RESULT AND DISCUSSION

A. Structural and morphological characterization

The pyramidal Ni sample obtained at 200 °C for 15 h in 60 mL glycerol is characterized by XRD, as shown in Fig. 1 (a). The diffraction peaks can be indexed to the fcc structure Ni (JCPDS 04-0850, $\alpha = 3.524$ Å),[18] indicating that single phase of nickel can be obtained under such condition.

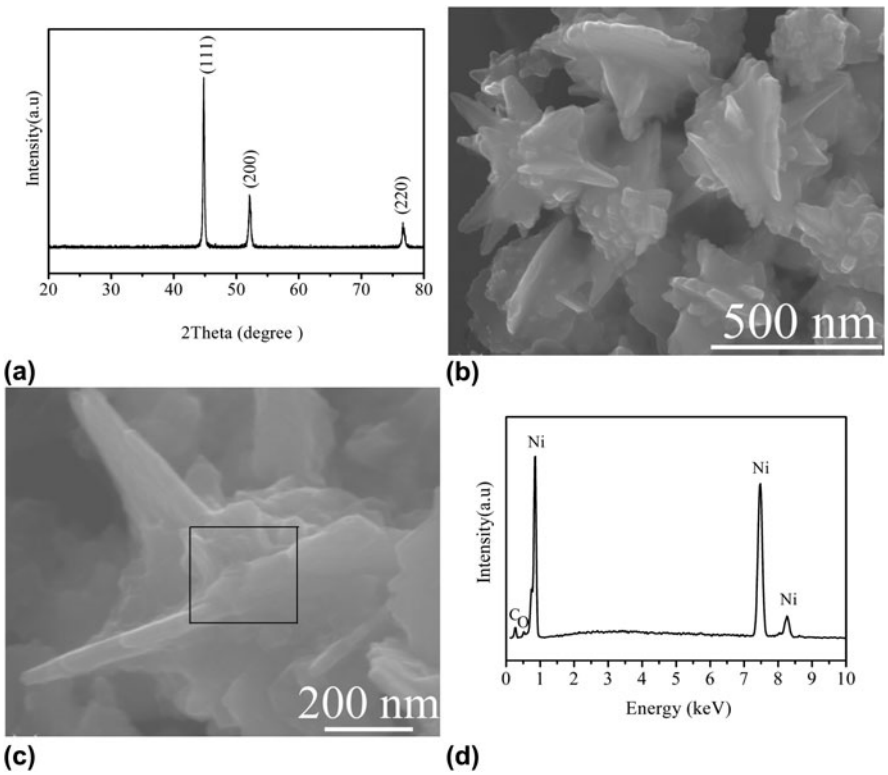


FIG. 1. (a) XRD pattern and (b) low-magnification, (c) high-magnification FESEM images of as-synthesized pyramidal Ni; (d) EDS pattern of the marked area in (c).

https://doi.org/10.1557/jmr.2014.151 Published online by Cambridge University Press

The field emission scanning electron microscopy (FESEM) images of the obtained products with different magnifications are presented in Figs. 1(b) and 1(c). Figure 1(b) is the overall morphology of the sample, which indicates the as-prepared products consist of pyramidal superstructures with the average diameter of about 1–2 μm. The magnified SEM image in Fig. 1(c) indicates that the superstructures comprise dozens of cones radiating from the center. The length of cone ranges from 200 to 600 nm. EDS spectrum of as-prepared Ni samples was shown in Fig. 1(d). EDS analysis of the prepared products confirms the Ni element, consistent with the XRD results. The occurrence of C peak in the EDS spectrum comes from the carbon conductive tape for supporting the samples during the test or some organic derivant products.

FTIR technique is used to detect the surface state of Ni cones, as shown in Fig. 2(a). The emerged peaks at 2924 and 2851 cm^{-1} are the vibration of C–H bond in a methyl group.[19] The absorption centered at 1618 cm^{-1} is corresponding to the hydrogen bonded O–H stretching. The bands at 1462 cm^{-1} is ascribed to the symmetric stretching vibration of carboxyl group.[20] The appearance of adsorption peak at 1116 cm^{-1} is ascribed to the C–O–H stretching vibration. The occurrence at 806 cm^{-1} is attributed to the C–H out-of-plane ring deformation vibration. The absorptions of 586 cm^{-1} is contributed to the vibrations of Ni–O bonds.[21] From above analysis, we can deduce that there are organic derivant and NiO on the surface of Ni cones. The oxidization stability of pyramidal Ni has also been characterized with TG [Fig. 2(b)]. The TG curve of Ni indicates that there are one weight loss and one weight gain. The drop of approximately 9.93% from room temperature to 390 °C is attributed to the removal of absorbed H_2O, glycerol and pyrolysis of organics on the particle surface.[21] The weight gain of 21.32% is due to the oxidation of Ni to NiO, started at 390 °C and stopped at 680 °C. It can be calculated that the Ni content is approximately 70.45% in the as-prepared Ni cones. The pyramidal Ni presents better oxidization stability than that of previously reported papers.[21,22]

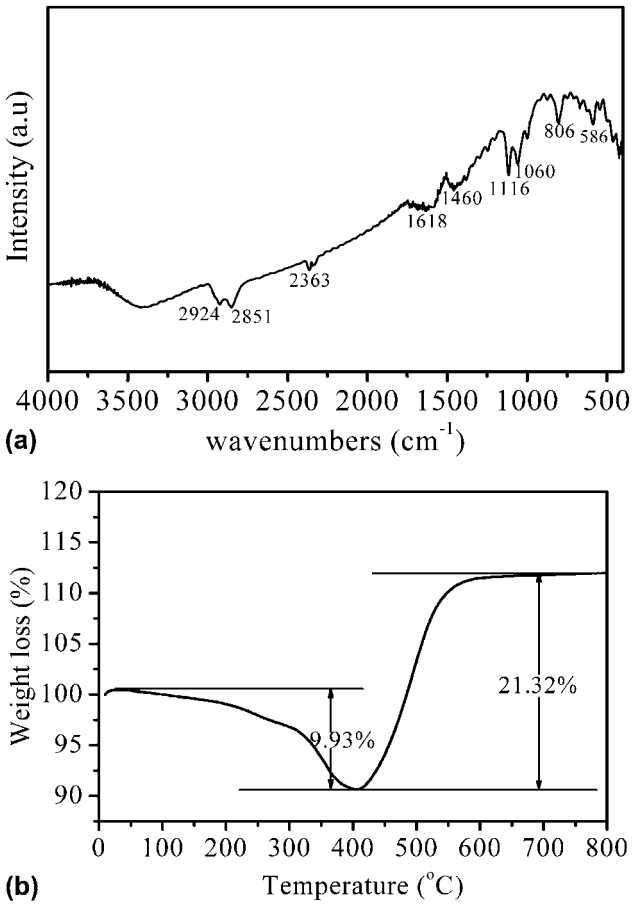


FIG. 2. (a) FTIR pattern and (b) TG curve of the as-received Ni products.

In liquid chemistry reaction systems, solvent plays a crucial role in determining the morphology of final products.[23,24] In this work, amounts of water are introduced in the polyol reduction system. It is revealed that the volume ratios of glycerol to water have a great effect on the morphology of the obtained products, while the total of amount of solvents is kept at 60 mL. Figure 3(a) shows that the as-received products at various volume ratios of glycerol to water are all metallic nickel. When the volume ratio of glycerol to water is 20:40, the resultant product presents irregular polyhedron structures, along with some quasi-microspheres [Fig. 3(b)]. With increasing the volume ratio to 30:30, the final products consist of irregular polyhedron and a minor amount of pyramidal structures [Fig. 3(c)]. When the volume ratio is further increased to 40:20, the obtained products mostly exhibit pyramidal structures [Fig. 3(d)]. From above analysis, it can be noted that the shapes of final products transform from irregular polyhedrons to pyramidal structures by increasing the amount of glycerol. Solvent can influence the reactivity, diffusion, and solubility behavior of the reagents, and thus influence the growth and morphologies of final products. The viscosity ranking of water and glycerol is $\upsilon_{water} < \upsilon_{glycerol}$, to some extent, higher viscosity can slow down the growth rate and benefit the isotropic growth.[24] On the other hand, glycerol with higher viscosity restrained the diffusion of Ni nuclei and resulted in the formation of pyramidal crystals.[25]

In addition, the volume ratios of glycerol to water and the amounts of NaOH have significant effects on morphologies of the final Ni products. The XRD pattern in Fig. 4(a) reveals that the obtained products are single phase of metallic Ni under different concentrations of NaOH. The SEM images in Fig. 4(b)–4(d) show typical morphologies of three samples obtained at different alkali concentrations with the other reaction conditions constant. At a low NaOH concentration of 0.025 mol, the product exhibits quasiflowerlike crystallites with average diameter of 1–2 μm [Fig. 4(b)]. When the NaOH concentration

https://doi.org/10.1557/jmr.2014.151 Published online by Cambridge University Press

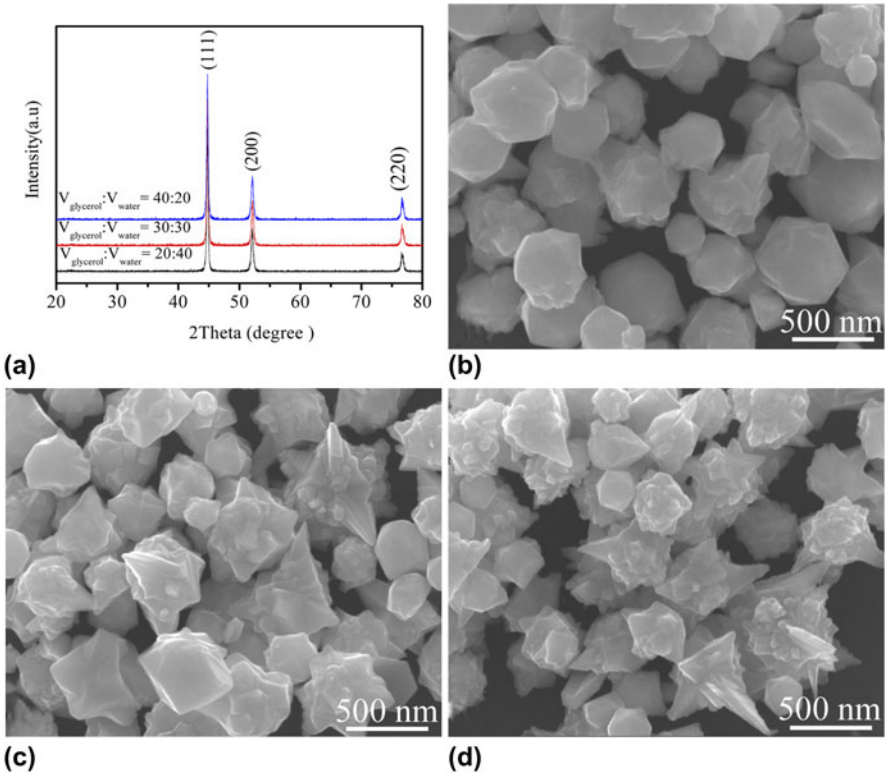


FIG. 3. (a) XRD patterns and (b–d) SEM images of the products obtained from the solvent with different volume ratios of glycerol to water: (b) 20:40, (c) 30:30, (d) 40:20.

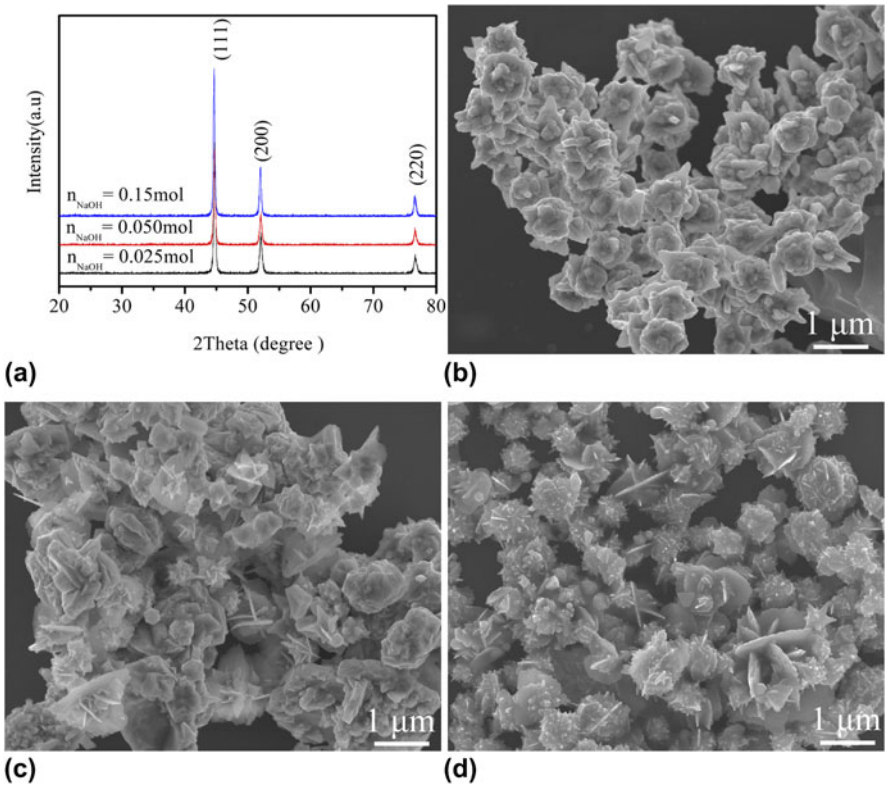


FIG. 4. (a) XRD patterns and (b–d) SEM images of the as-prepared Ni samples produced at the different concentration of NaOH (b) 0.025 mol, (c) 0.05 mol, (d) 0.15 mol.

https://doi.org/10.1557/jmr.2014.151 Published online by Cambridge University Press

reached 0.05 mol, the product consisted of irregular granules and flowerlike crystallites [Fig. 4(c)]. When the NaOH concentration was further increased to 0.15 mol, the product becomes a mixture of urchinlike and flowerlike Ni particles [Fig. 4(d)]. When NaOH concentration is 0, the Ni^{2+} ions still could not be reduced by glycerol even though reaction time is prolonged up to 48 h (not shown here). It is confirmed that NaOH has two meaningful roles during the polyol reduction process.[23,26] On the one hand, the reducing ability of polyol can be enhanced with increasing alkalinity, thus it can accelerate the reduction of metal ions.[27] On the other hand, high NaOH concentration can decrease Ni^{2+} concentration in the solution and subsequently slow down the reduction reaction. The morphology evolution process mentioned above indicates that a suitable NaOH concentration can effectively control the producing rate of nickel atoms, thus kinetically control the aggregation and growth of the nickel crystallites and further determine the morphology of final products.[22,28]

B. Dielectric and dynamic magnetic properties

The electromagnetic wave absorption property of materials is generally determined by the complex relative permittivity and permeability as well as the tangent loss (dielectric tangent loss: $\tan\delta_\varepsilon = \varepsilon''/\varepsilon'$; magnetic tangent loss: $\tan\delta_\mu = \mu''/\mu'$). The electromagnetic parameters (relative complex permittivity, ε_r, and relative complex permeability, μ_r) of the wax composites containing 70 wt% of the pyramidal Ni were measured at the range of 1.0–18.0 GHz for the investigation of electromagnetic (EM) absorption properties of the obtained products. As it is well known, the real permittivity (ε') and real permeability (μ') symbolize the storage ability of electromagnetic energy, while the imaginary permittivity (ε'') and imaginary permeability (μ'') are related to the dissipation of electromagnetic energy.[29] Fig. 5(a) shows the frequency dependence of the real part (ε') and imaginary part (ε'') of relative complex permittivity ($\varepsilon_r = \varepsilon' - j\varepsilon''$) of the composites. The ε' value is in the range of 10.30–11.76 and the ε'' value is in the range of 0.53–2.01. Compared with the Ni octahedra or hollow microspheres as reported in the literatures,[13,30] the Ni submicrometer horns have relatively low ε' values. This is advantageous for keeping a good impedance matching between the composites based on Ni submicrometer horns and free space, thus consequently decreasing the reflection coefficient for EM waves. The real part (μ') and the imaginary part (μ'') of the relative permeability are plotted as a function of frequency in Fig. 5(b). It indicates that the μ' values gradually decrease from 2.00 to 0.86 over the whole frequency range of 1.0–18.0 GHz. Meanwhile, the image part (μ'') is in the range of 0.02–0.62 over 1.0–18.0 GHz. The imaginary part of relative permeability (μ'') exhibited a broad peak in the 2.0–8.0 GHz range with a maximum point of 0.62 at 4.8 GHz, which may be ascribed to the natural resonance of pyramidal Ni structure.

In general, the excellent EM wave absorptions are strongly dependent on the efficient complementarities between the relative permeability and permittivity. If there is only dielectric loss or only magnetic loss, the EM attenuation will be very weak.[31] Therefore, the dielectric

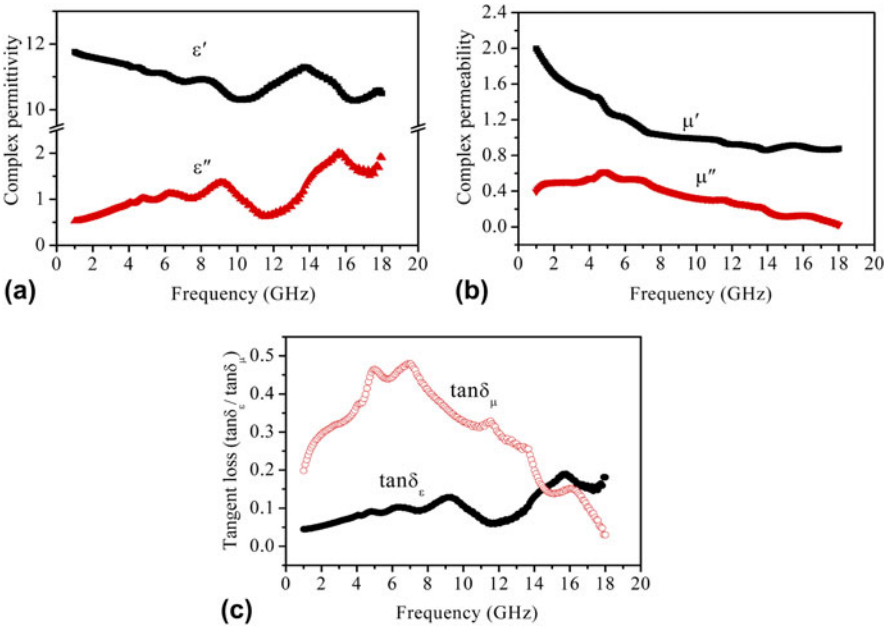


FIG. 5. (a) Frequency dependence of complex relative permittivity, and (b) permeability, and (c) tangent loss for the paraffin-based composites containing 70 wt% pyramidal Ni.

https://doi.org/10.1557/jmr.2014.151 Published online by Cambridge University Press

tangent loss ($\tan\delta_\varepsilon$) and the magnetic tangent loss ($\tan\delta_\mu$) were calculated based on the data [Figs. 5(a) and 5(b)] and the results are shown in Fig. 5(c). The values of $\tan\delta_\varepsilon$ are 0.04–0.15 between 1.0 and 14.6 GHz, whereas those of $\tan\delta_\mu$ are 0.15–0.48 between 1.0 and 14.6 GHz. This reveals that the magnetic loss plays main role in the EM absorption below 14.6 GHz, whereas the dielectric loss becomes dominant at high-frequency range. Therefore, effective complementarities between the dielectric loss and magnetic loss are realized, suggesting that these submicrometer Ni cones have excellent EM wave absorption properties.

To reveal the mechanism of dielectric loss, the complex permittivity has been analyzed according to the Debye dipolar relaxation model. The Debye dipolar relaxation of dielectric oxide can be expressed as:

$$(\varepsilon' - \varepsilon_\infty)^2 + (\varepsilon'')^2 = (\varepsilon_s - \varepsilon_\infty)^2 \quad , \qquad (1)$$

where ε_s and ε_∞ are stationary dielectric constant and optical dielectric constant, respectively.[32] Theoretically, the plot of ε' versus ε'' should be a single semicircle, which is usually defined as Cole–Cole semicircle.[33] Figure 6(a) shows the curve characteristics of ε' versus ε'' for the obtained sample. It is worth noting that the sample presents a clear segment of four overlapped semicircles. The presence of semicircles suggests that there are dual dielectric relaxation processes, and each semicircle corresponds to a Debye dipolar relaxation. The electrons that reside on the organic derivant may gain enough energy to surmount the interfaces among the organic derivant, wax and the pyramidal Ni, then move onto the Ni particles. Therefore, an interfacial behavior of accumulating space charges is expected for the composite, leading to a steady dielectric relaxation. However, the Cole–Cole semicircles are distorted, suggesting that besides the dielectric relaxation, other mechanisms such as the motion of conducting electrons and the particles/paraffin interfacial polarization may contribute to the permittivity spectra, too.[34] Thus the dielectric relaxation processes and interfacial polarization are expected to result in the enhancement of dielectric loss. Furthermore, the organic derivant leads to the changes of electronic spin and charge polarization of the as-received product, which further affects the complex permittivity.

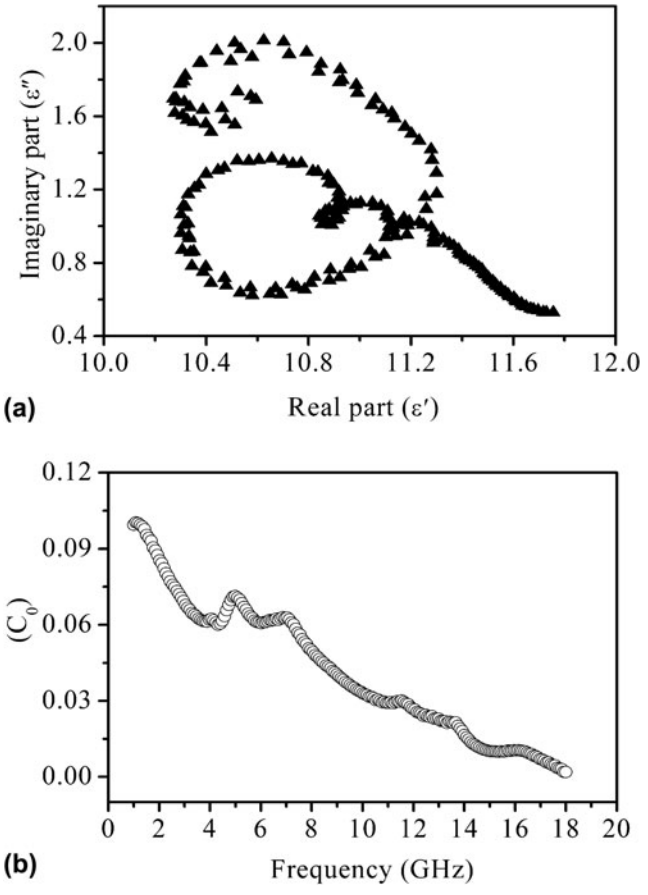


FIG. 6. (a) The relation between real part (ε') and imaginary part (ε'') of the complex permittivity (Cole–Cole plot). (b) The value C_0 of $\mu''(\mu')^{-2}f^{-1}$ as a function of frequency.

Generally, the microwave magnetic loss of magnetic particles originates from hysteresis, domain wall resonance, eddy current effect, natural resonance, and exchange resonance for the micro/nanostructure materials. In our case, the hysteresis loss is negligible in weak applied field.[35] The domain wall displacement loss occurs only in the MHz range rather than GHz, so the contribution of domain wall resonance can also be excluded.[36] The eddy current loss is related to the diameter of nanoparticles (d) and the electric conductivity (σ), which can be expressed by[37]

$$\mu'' \approx 2\pi\mu_0(\mu')^2\sigma d^2 f/3 \quad , \qquad (2)$$

where f is the applied frequency, μ_0 is the vacuum permeability. It is known from the above equation that, if magnetic loss only results from eddy current loss, the values of $C_0(C_0 = \mu''(\mu')^{-2}f^{-1} = 2\pi\mu_0\sigma d^2/3)$ should be constant by varying frequency, which is called the skin-effect criterion.[35] In pyramidal Ni, the values of C_0 decrease gradually with increasing frequency in the whole range of 1.0–18.0 GHz [Fig. 6(b)], the eddy current loss can be precluded, too. Thus, the magnetic loss should result from the nature resonance and exchange resonance.

C. Microwave absorbing properties

According to the measured data of permittivity and permeability, the RL usually can be evaluated by the following equation:[20]

$$\mathrm{RL} = 20\log_{10}|(Z_{in} - Z_0)/(Z_{in} + Z_0)| \quad , \qquad (3)$$

where Z_0 is the impedance of free space, and Z_{in} is the input characteristic impedance, which can be expressed as

https://doi.org/10.1557/jmr.2014.151 Published online by Cambridge University Press

$$Z_{in} = Z_0\sqrt{\frac{\mu_r}{\varepsilon_r}}\tanh\left(j\frac{2\pi fd\sqrt{\mu_r\varepsilon_r}}{c}\right) \quad , \qquad (4)$$

where μ_r is the complex permeability, ε_r is the complex permittivity, f is the frequency, c is the velocity of light, and d is the thickness of the composites.[38]

Figure 7(a) shows the calculated RL curves for the paraffin-based composites containing 70 wt% as-synthesized nickel cones with different thicknesses. The RL values of the wax composites less than −10 dB, which are comparable to 90% of EM wave absorption, were obtained in the range of 3.9–15.0 GHz with absorber thicknesses of 1.8–3.8 mm. It can be found that the minimum RL peak moves toward the lower frequency region with increasing thickness of the composite. It is worth noting that the composites with a thickness of 3.8 mm show a minimum RL value of −41.6 dB at 4.7 GHz. Figure 7(b) shows the bandwidth of the absorption frequency for RL < −10 dB in a two-dimensional contour plot. The result indicates that a thinner absorber layer has a wider frequency bandwidth. The enhanced EM wave absorption may be attributed to impedance match, and the cooperative effect between dielectric loss and magnetic loss. Apart from the dielectric loss and magnetic loss, the unique pyramidal structure is also beneficial for the enhancement of EM wave absorption. The pyramidal structure of nickel contributes to the polarization of electrical charge. The special morphology can form anisotropic antennas and discontinuous networks in the composites. Similar behavior ascribed to high aspect ratio has been observed in copper and magnetic microwire-based composites.[39–41] It is available for the EM wave to penetrate the composites formed by the numerous conductive Ni cones and the energy will be induced into dissipative current. Therefore, EM waves will be consumed in the discontinuous networks, which lead to the energy attenuation.[42] Ni horns not only lead to diffuse scattering of the incident microwaves, which results in the attenuation of EM energy, but also act as receivers of microwaves, which can produce vibrating microcurrent in the local networks and this microcurrent will be exhausted. Some works related with graphite flakes shown an equivalent behavior where a dihedral angle where the microwave reflects many times resulting in the lots of electromagnetic wave energy.[43] Besides above mentioned reasons for EM absorption, the electromagnetic wave can be absorbed via the "geometrical effect", which means that when the thickness of absorber satisfies the equation[38,44]

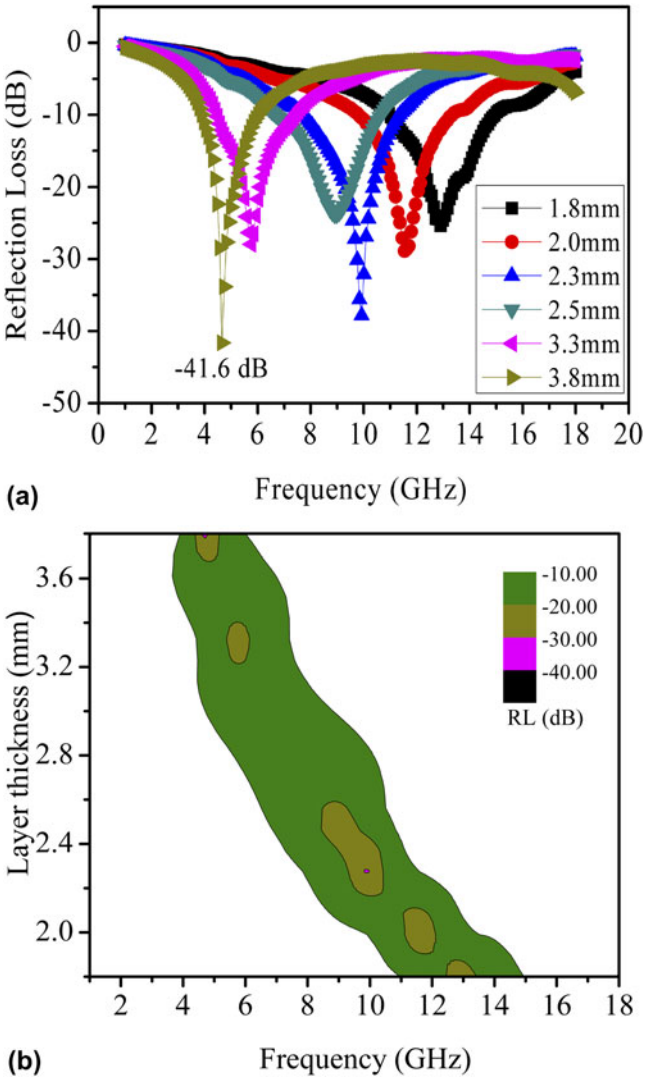


FIG. 7. (a) Frequency dependence of the microwave RL and (b) contour map of the bandwidth with RL < −10 dB (90% absorption) as a function of the absorber thickness.

$$d = \frac{l\lambda_m}{4}(l = 1, 3, 5, \ldots) \quad , \qquad (5)$$

$$\lambda_m = \frac{\lambda_0}{\sqrt{|\mu_r||\varepsilon_r|}} \quad , \qquad (6)$$

where λ_m is the wavelength at certain frequency, $|\mu_r|$ and $|\varepsilon_r|$ are the moduli of μ_r and ε_r, and λ_0 is the wavelength in the free space, the incident and reflected waves in the absorber are out of phase 180° and resulting the reflected waves in the air–absorber interface are totally canceled. We propose that the geometrical effect plays an important role in microwave absorption of pyramidal Ni. At matching frequency f_m = 4.7 GHz, by substituting the values of $\varepsilon_r = 11.25 - j1.01$, and $\mu_r = 1.41 - j0.61$ into Eq. (5) with l = 1, we can get a matching thickness d = 3.84 mm, which is perfectly consistent to the thickness of 3.8 mm in the real measurement. Hence the above calculation validates our supposition that the strong microwave absorbing ability of Ni cones also arises from geometrical effect.

https://doi.org/10.1557/jmr.2014.151 Published online by Cambridge University Press

IV. CONCLUSION

In summary, the pyramidal Ni structures have been successfully synthesized via a facile template-free and glycerol-assist solvothermal method without surfactants or complex precursors. The glycerol served as both reducing agent and solvent in this synthesis. The influence of concentrations of NaOH and volume ratios of glycerol to water on the morphologies was investigated in detail. The paraffin-based composites containing 70 wt% Ni submicrometer cones show good electromagnetic wave absorbing characteristics and the RL values less than −10 dB are obtained in the frequency range of 3.9–15.0 GHz with corresponding absorber thicknesses of 1.8–3.8 mm. The pyramidal Ni exhibited a minimum RL value of −41.6 dB at 4.7 GHz. Such excellent microwave absorbing performance is attributed to synergic effect between dielectric loss and magnetic loss, geometrical effect and unique morphology. The results demonstrate that the Ni submicrometer cones obtained by the simple glycerol reduced method have a good application as a strong-absorption, thin-thickness, wideband and low-cost microwave absorber.

REFERENCES

1. G. Tong, W. Wu, R. Qiao, J. Yuan, J. Guan, and H. Qian: Morphology dependence of static magnetic and microwave electromagnetic characteristics of polymorphic Fe_3O_4 nanomaterials. *J. Mater. Res.* **26**, 1639 (2011).
2. G. Tong, J. Ma, W. Wu, Q. Hua, R. Qiao, and H. Qian: Grinding speed dependence of microstructure, conductivity, and microwave electromagnetic and absorbing characteristics of the flaked Fe particles. *J. Mater. Res.* **26**, 682 (2011).
3. Y-X. Gong, L. Zhen, J-T. Jiang, C-Y. Xu, W-S. Wang, and W-Z. Shao: Synthesis of Fe-ferrite composite nanotubes with excellent microwave absorption performance. *CrystEngComm* **13**, 6839 (2011).
4. L. Du, Y. Du, Y. Li, J. Wang, C. Wang, X. Wang, P. Xu, and X. Han: Surfactant-assisted solvothermal synthesis of $Ba(CoTi)_xFe_{12-2x}O_{19}$ nanoparticles and enhancement in microwave absorption properties of polyaniline. *J. Phys. Chem. C* **114**, 19600 (2010).
5. Q. Hu, G. Tong, W. Wu, F. Liu, H. Qian, and D. Hong: Selective preparation and enhanced microwave electromagnetic characteristics of polymorphous ZnO architectures made from a facile one-step ethanediamine-assisted hydrothermal approach. *CrystEngComm* **15**, 1314 (2013).
6. F. Du, G. Tong, C. Tong, Y. Liu, and J. Tao: Selective synthesis and shape-dependent microwave electromagnetic properties of polymorphous ZnO complex architectures. *J. Mater. Res.* **29**, 649 (2014).
7. C. He, S. Qiu, X. Wang, J. Liu, L. Luan, W. Liu, M. Itoh, and K-i. Machida: Facile synthesis of hollow porous cobalt spheres and their enhanced electromagnetic properties. *J. Mater. Chem.* **22**, 22160 (2012).
8. C. Gong, J. Zhang, X. Zhang, L. Yu, P. Zhang, Z. Wu, and Z. Zhang: Strategy for ultrafine Ni fibers and investigation of the electromagnetic characteristics. *J. Phys. Chem. C* **114**(22), 10101 (2010).
9. Z. Yu, Z. Yao, N. Zhang, Z. Wang, C. Li, X. Han, X. Wu, and Z. Jiang: Electric field-induced synthesis of dendritic nanostructured α-Fe for electromagnetic absorption application. *J. Mater. Chem. A* **1**, 4571 (2013).
10. J. Wu and L. Kong: High microwave permittivity of multiwalled carbon nanotube composites. *Appl. Phys. Lett.* **84**, 4956 (2004).
11. Z. Wang, L. Wu, J. Zhou, W. Cai, B. Shen, and Z. Jiang: Magnetite nanocrystals on multiwalled carbon nanotubes as a synergistic microwave absorber. *J. Phys. Chem. C* **117**, 5446 (2013).
12. G. Tong, F. Liu, W. Wu, F. Du, and J. Guan: Rambutanlike Ni/MWCNT heterostructures: Easy synthesis, formation mechanism, and controlled static magnetic and microwave electromagnetic characteristics. *J. Mater. Chem. A* **2**, 7373 (2014) DOI: 10.1039/c4ta00117f.
13. G. Tong, Q. Hu, W. Wu, W. Li, H. Qian, and Y. Liang: Submicrometer-sized NiO octahedra: Facile one-pot solid synthesis, formation mechanism, and chemical conversion into Ni octahedra with excellent microwave-absorbing properties. *J. Mater. Chem.* **22**, 17494 (2012).
14. G. Sun, B. Dong, M. Cao, B. Wei, and C. Hu: Hierarchical dendrite-like magnetic materials of Fe_3O_4, γ-Fe_2O_3, and Fe with high performance of microwave absorption. *Chem. Mater.* **23**, 1587 (2011).
15. B. Gao, L. Qiao, J. Wang, Q. Liu, F. Li, J. Feng, and D. Xue: Microwave absorption properties of the Ni nanowires composite. *J. Phys. D: Appl. Phys.* **41**, 235005 (2008).
16. Z. Wang, J. Zou, Z. Ding, J. Wu, P. Wang, S. Jin, and H. Bi: Magnetic and microwave absorption properties of Ni microcrystals with hierarchical branch-like and flowers-like shapes. *Mater. Chem. Phys.* **142**, 119 (2013).
17. T. Liu, P. Zhou, J. Xie, and L. Deng: Electromagnetic and absorption properties of urchinlike Ni composites at microwave frequencies. *J. Appl. Phys.* **111**, 093905 (2012).
18. X. Ni, Q. Zhao, H. Zheng, B. Li, J. Song, D. Zhang, and X. Zhang: A novel chemical reduction route towards the synthesis of crystalline nickel nanoflowers from a mixed source. *Eur. J. Inorg. Chem.* **2005**, 4788 (2005).
19. S. Carenco, C. Boissière, L. Nicole, C. Sanchez, P. Le Floch, and N. Mézailles: Controlled design of size-tunable monodisperse nickel nanoparticles. *Chem. Mater.* **22**, 1340 (2010).
20. T. Chen, F. Deng, J. Zhu, C. Chen, G. Sun, S. Ma, and X. Yang: Hexagonal and cubic Ni nanocrystals grown on graphene: Phase-controlled synthesis, characterization and their enhanced microwave absorption properties. *J. Mater. Chem.* **22**, 15190 (2012).
21. H. Wang, X. Jiao, and D. Chen: Monodispersed nickel nanoparticles with tunable phase and size: Synthesis, characterization, and magnetic properties. *J. Phys. Chem. C* **112**, 18793 (2008).
22. Z. An, S. Pan, and J. Zhang: Synthesis and tunable assembly of spear-like nickel nanocrystallites: From urchin-like particles to prickly chains. *J. Phys. Chem. C* **113**, 1346 (2009).
23. J. Guan, L. Liu, L. Xu, Z. Sun, and Y. Zhang: Nickel flower-like nanostructures composed of nanoplates: One-pot synthesis, stepwise growth mechanism and enhanced ferromagnetic properties. *CrystEngComm* **13**, 2636 (2011).
24. L. Zhao, H. Zhang, Y. Xing, S. Song, S. Yu, W. Shi, X. Guo, J. Yang, Y. Lei, and F. Cao: Morphology-controlled synthesis of magnetites with nanoporous structures and excellent magnetic properties. *Chem. Mater.* **20**, 198 (2007).
25. X. Ni, Y. Zhang, J. Song, and H. Zheng: Solvent mediated assembly of nickel crystallites: From chains to isolated spheres. *J. Cryst. Growth* **299**, 365 (2007).
26. R.J. Joseyphus, T. Matsumoto, H. Takahashi, D. Kodama, K. Tohji, and B. Jeyadevan: Designed synthesis of cobalt and its alloys by polyol process. *J. Solid State Chem.* **180**, 3008 (2007).
27. D. Ung, G. Viau, C. Ricolleau, F. Warmont, P. Gredin, and F. Fiévet: CoNi nanowires synthesized by heterogeneous nucleation in liquid polyol. *Adv. Mater.* **17**, 338 (2005).

https://doi.org/10.1557/jmr.2014.151 Published online by Cambridge University Press

28. X. Ni, Q. Zhao, D. Zhang, X. Zhang, and H. Zheng: Novel hierarchical nanostructures of nickel: Self-assembly of hexagonal nanoplatelets. *J. Phys. Chem. C* **111**, 601 (2006).
29. W. Zhou, X. Hu, X. Bai, S. Zhou, C. Sun, J. Yan, and P. Chen: Synthesis and electromagnetic, microwave absorbing properties of core–shell Fe_3O_4–poly(3, 4-ethylenedioxythiophene) microspheres. *ACS Appl. Mat. Interfaces* **3**, 3839 (2011).
30. Y. Deng, X. Liu, B. Shen, L. Liu, and W. Hu: Preparation and microwave characterization of submicrometer-sized hollow nickel spheres. *J. Magn. Magn. Mater.* **303**, 181 (2006).
31. Y-J. Chen, P. Gao, R-X. Wang, C-L. Zhu, L-J. Wang, M-S. Cao, and H-B. Jin: Porous Fe_3O_4/SnO_2 core/shell nanorods: Synthesis and electromagnetic properties. *J. Phys. Chem. C* **113**, 10061 (2009).
32. P. Xu, X. Han, C. Wang, D. Zhou, Z. Lv, A. Wen, X. Wang, and B. Zhang: Synthesis of electromagnetic functionalized nickel/polypyrrole core/shell composites. *J. Phys. Chem. B* **112**, 10443 (2008).
33. P.H. Fang: Cole–Cole diagram and the distribution of relaxation times. *J. Chem. Phys.* **42**, 3411 (1965).
34. N. Pinna, S. Grancharov, P. Beato, P. Bonville, M. Antonietti, and M. Niederberger: Magnetite nanocrystals: Nonaqueous synthesis, characterization, and solubility. *Chem. Mater.* **17**, 3044 (2005).
35. M. Wu, Y.D. Zhang, S. Hui, T.D. Xiao, S. Ge, W.A. Hines, J.I. Budnick, and G.W. Taylor: Microwave magnetic properties of $Co_{50}/(SiO_2)_{50}$ nanoparticles. *Appl. Phys. Lett.* **80**, 4404 (2002).
36. S. Gangopadhyay, G.C. Hadjipanayis, B. Dale, C.M. Sorensen, K.J. Klabunde, V. Papaefthymiou, and A. Kostikas: Magnetic properties of ultrafine iron particles. *Phys. Rev. B* **45**, 9778 (1992).
37. J. Guo, X. Wang, P. Miao, X. Liao, W. Zhang, and B. Shi: One-step seeding growth of controllable Ag@Ni core-shell nanoparticles on skin collagen fiber with introduction of plant tannin and their application in high-performance microwave absorption. *J. Mater. Chem.* **22**, 11933 (2012).
38. P. Marín, D. Cortina, and A. Hernando: Electromagnetic wave absorbing material based on magnetic microwires. *IEEE Trans. Magn.* **44**, 3934 (2008).
39. A. Gorriti, P. Marín, D. Cortina, and A. Hernando: Microwave attenuation with composite of copper microwires. *J. Magn. Magn. Mater.* **322**, 1505 (2010).
40. M. Han, D. Liang, and L. Deng: Fabrication and electromagnetic wave absorption properties of amorphous $Fe_{79}Si_{16}B_5$ microwires. *Appl. Phys. Lett.* **99**, 082503 (2011).
41. P. Marín, D. Cortina, and A. Hernando: High frequency magnetic behavior of magnetic microwires. *J. Magn. Magn. Mater.* **290–291**, 1957 (2005).
42. R.F. Zhuo, H.T. Feng, J.T. Chen, D. Yan, J.J. Feng, H.J. Li, B.S. Geng, S. Cheng, X.Y. Xu, and P.X. Yan: Multistep synthesis, growth mechanism, optical, and microwave absorption properties of ZnO dendritic nanostructures. *J. Phys. Chem. C* **112**, 11767 (2008).
43. R.F. Zhuo, L. Qiao, H.T. Feng, J.T. Chen, D. Yan, Z.G. Wu, and P.X. Yan: Microwave absorption properties and the isotropic antenna mechanism of ZnO nanotrees. *J. Appl. Phys.* **104**, 094101 (2008).
44. C. Wang, X. Han, P. Xu, J. Wang, Y. Du, X. Wang, W. Qin, and T. Zhang: Controlled synthesis of hierarchical nickel and morphology-dependent electromagnetic properties. *J. Phys. Chem. C* **114**, 3196 (2010).

https://doi.org/10.1557/jmr.2014.151 Published online by Cambridge University Press